Egypt. J. Chem. **Vol. 68**, No. 3 pp. 131 - 144 (2025)

Egyptian Journal of Chemistry

http://ejchem.journals.ekb.eg/

Development of a Quartz Crystal Microbalance-Based Nano Cobalt Sensor for Rapid Detection of Methylene Blue in Water Streams

Shaimaa. M. Elgazar [1*], Abeer Taha Ibrahium[1], Walaa H. Mahmoud[1], Ahmed A. El-Sherif[1]

[1]*Chemistry Department, Faculty of Science, Cairo University, Giza, 12613 Egypt*

Abstract

The dyeing processes in the textile industry give rise to dyes that function as environmental pollutants, contributing to the discoloration of wastewater and posing various ecological concerns. Researchers are actively developing versatile nanosensors in the rapidly advancing field of nanotechnology. These nanosensors show potential in detecting azo-toxic dyes present in food products, offering a wide scope for future innovations in sensor design. This comprehensive review explores various types of nanosensors, emphasizing their crucial roles in sensing and their specific applications for the detection of azo-toxic dyes. The advantages of nanosensors over traditional sensing methods, their diverse applications utilizing nanomaterials, and the potential health implications of azo dyes on human well-being are discussed. The review outlines key parameters for determining permissible limits and recommends an Acceptable Daily Intake (ADI) for azo-toxic dyes. A noteworthy technique in this context is the Quartz Crystal Microbalance (QCM), which leverages the sensitivity of resonant crystal frequency to quantify dye concentrations precisely. Experimental results conclusively demonstrate the proficiency of the QCM method in providing both quantitative and qualitative analyses of dyes in real-time settings within wastewater. A groundbreaking advancement involves a novel nanosensor employing cobalt nanoparticles to detect Methylene Blue (MB) dye simultaneously. The complex characterization of this nano cobalt sensor utilized various analytical tools, including Dynamic Light Scattering (DLS), Zeta potential analysis, Atomic Force Microscopy (AFM), Fourier-Transform Infrared Spectroscopy (FT-IR), as well as BET surface area and pore size determination. Furthermore, the mechanical stability of the sensor was affirmed through the investigation of the applied ionophore's lipophilicity using contact angle measurements, revealing an average contact angle of 120.70°. This attribute significantly contributes to the robustness of the sensor. The sensor's responsiveness was carefully monitored under varying pH and temperature conditions. The proposed sensor exhibited rapid and sensitive responses, even at very low dye concentrations (0.1 ppm), with a swift response time of 8-10 minutes.

Keywords: Nanosensor; Nano complex; Toxic dyes; AFM; BET; FT-IR

1. **Introduction**

In the realm of sensor advancement, a critical imperative exists to progress processing methodologies for the deliberate construction of specific morphologies and nanostructures in nanomaterials. These nanostructures play a pivotal role in influencing the performance of nanomaterials, underscoring their paramount significance[1]. Integrating nanoscale materials into sensing applications is expanding substantially, with nanosensors progressively assuming pivotal roles across diverse sectors such as environmental assessment, pathogen identification, and biomedical diagnostics[2]. The domain of nanomaterial-enabled sensors stands as a captivating technological frontier, facilitating remarkably precise detection within the nanomolar to sub-picomolar range for environmental contaminants. The appeal of these sensors is rooted in their potential to facilitate seamless, in-field detection of contaminants, eliminating the necessity for intricate laboratory apparatus[3]. Nanomaterials have catalyzed groundbreaking advancements in sensor design by enabling miniaturization, enhancing portability, and accelerating signal response times[4]. The remarkably high surface area-to-volume ratios of nanomaterials, combined with their facile surface modification capabilities, make them exceptionally responsive to alterations in surface chemistry[5]. This distinctive attribute empowers nanosensors to achieve unprecedentedly low detection thresholds. Noteworthy is the fact that, in specific instances, the heightened sensitivity of nano-enabled sensors can be attributed to the size similarity of nanomaterials to the target analytes (e.g., metal ions, pathogens, biomolecules, antibodies, DNA), enabling exploration of previously inaccessible matrices[6][7]. The Quartz Crystal Microbalance (QCM) technology is a highly promising sensor technology that offers several advantages, such as cost-effectiveness, rapid responsiveness, portability, label-free real-time operation, and notable sensitivity. As a result, it is very well-suited for online detection of analytes with high precision. This makes it a considerable candidate for the development of advanced sensor systems in the future[8]. In our ongoing scientific pursuits, our primary emphasis lies in developing a comprehensive analytical sensor specifically tailored for

*Corresponding author e-mail: shaimaa.mostafa.elgazar@gmail.com.; (Shaimaa M. Elgazar).
Received date 15 May 2024; Revised date 23 July 2024; Accepted date 28 July 2024
DOI: 10.21608/EJCHEM.2024.290034.9717

studying dyes, as exemplified by the case of methylene blue dye. The innovative detection system under development offers rapid and precise determinations of dye concentrations with minimal sample preparation or the need for constant instrument supervision.

.

2. Materials and Methods

2.1. Experimental

2.1.1. Preparation of Nano cobalt complex.

The nano cobalt complex was synthesized through a meticulous procedure involving the amalgamation of a heated ethanolic solution (maintained at 70°C)[9], [10] comprising the Schiff base ligand (0.4 g (1.53 mmol)) (refer to Fig 1) with a heated solution of metal salt ((1.53 mmol) $CoCl_2.6H_2O$) in absolute ethanol (20 ml) [13]. Following a stirring duration of 5 hours under reflux conditions, the resultant complex precipitated (Scheme1). The obtained precipitates were methodically collected via filtration, subjected to repeated washing, and ultimately dried under vacuum conditions using anhydrous calcium chloride[11]. This systematic approach ensured the attainment of a highly pure metal complex, which further underwent recrystallization. Notably, the ensuing complex experienced a 15-minute treatment with an ultrasonic probe, inducing a distinctive color transformation from dark brown to a profound golden-brown hue[12], [13].

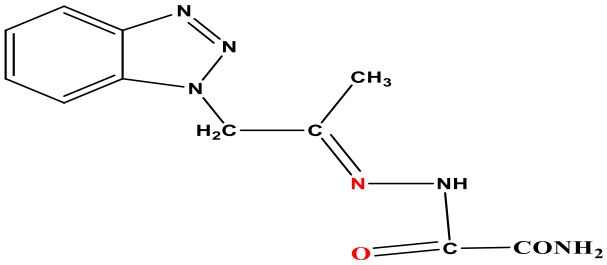

(*E*)-2-(2-(1-(1*H*-benzo[*d*][1,2,3]triazol-1-yl)propan-2-ylidene)hydrazineyl)-2-oxoacetamide

Fig. 1. Schiff base ligand (L)

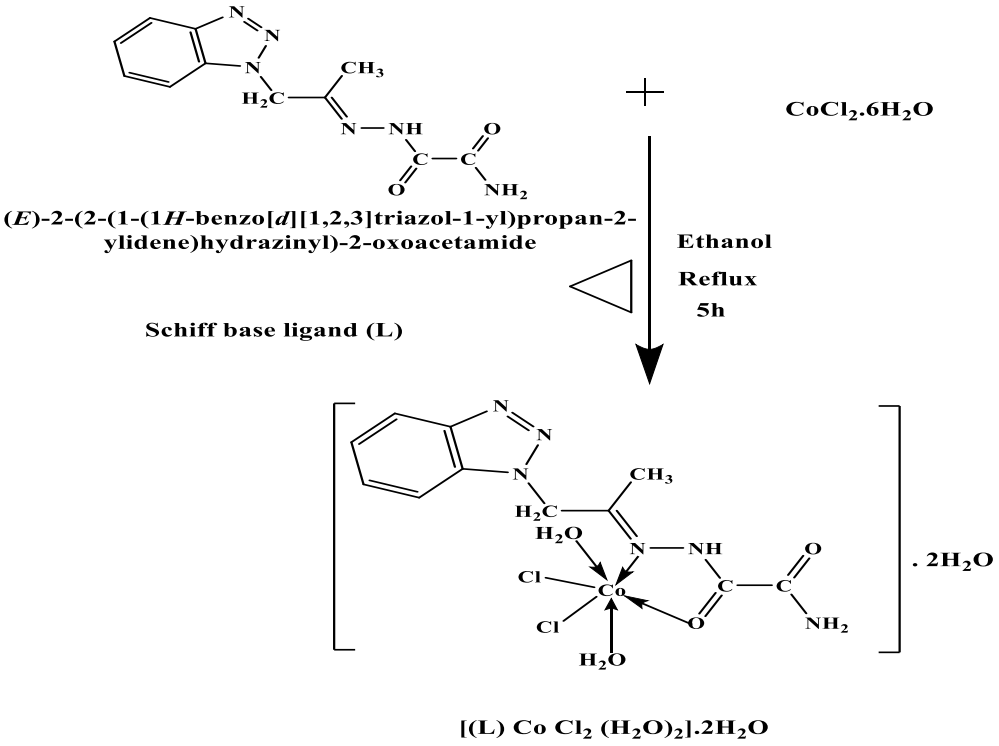

Scheme 1. Schiff base Cobalt Complex Pathway formation

2.1.2. Instrumentation

The elemental composition analysis of carbon, hydrogen, and nitrogen was conducted utilizing a CHNS-932 (LECO) Vario Elemental analyzer at the Microanalytical Center, Cairo University, Egypt [14]. The determination of melting points was achieved using the triforce XMTD-3000 apparatus [15]. Fourier transform infrared (FT-IR) spectra were recorded using a Perkin-Elmer 1650 spectrometer with KBr disks in the spectral range of 4000–400 cm^{-1} [16]. Molar conductance measurements of solid complex solutions in ethanol at 10−3 M concentrations were performed using a Jenway 4010 conductivity meter [17-19]. Mass spectra via the electron ionization method at 70 eV [20,21] were acquired using an MS-5988 GS-MS Hewlett-Packard instrument. UV-Vis spectra spanning wavelengths from 200 to 700 nm [22] were generated using a Perkin-Elmer Model Lambda 20 automated spectrophotometer. Antimicrobial investigations were conducted at the Microanalytical Center, Cairo University [23], and cytotoxicity assessments were conducted at the National Cancer Institute, Cairo University [24]. To determine the surface charge and particle size of the nano cobalt complex, zeta potential was measured using a ZetaSizer instrument (NanoSight NS500, Malvern Panalytical, Malvern, UK) [25]. Surface area and pore volume were quantified using a surface area and pore volume analyzer (Quanta Chrome, Nova Touch 4L, USA) employing the BET multi-point and DH pore volume methods [26]. A degassing process at 65°C for 1.25 hours was performed for the metal complex nanoparticles. Atomic Force Microscopy (AFM) studies were conducted using an AFM instrument manufactured by Oxford company, the Jupiter XR AFM model [27], to discern the morphology of the cobalt complex nanoparticles. BeforeAFM analysis, a 15-minute sonication was conducted using an ultrasonic probe sonicator (UP400S, Hielscher, Oderstraße, Teltow, Germany) at a frequency of 55 kHz, an amplitude of 55%, and a cycle of 0.55. Thin films were synthesized using a Spain coater instrument (Laurell-650Sz, France) under vacuum conditions, with a rotational speed of 750 rpm and a droplet rate of 50 µm per 120 seconds. AFM images and roughness profiles were obtained at 47 nm x 47 nm using a gold-coated cantilever in contact mode with a scanning speed of 0.31 µm/s [27]. Wettability assessment was conducted using a Biolin Scientific contact angle analyzer (model T200). The sessile drop condition was maintained with a measurement time of 10 seconds. Distilled water (4 µm) was used to determine the surface's wettability [28].

2.1.3.Establishing of QCM-Based cobalt complex Nanosensors

The QCM sensor utilized in this study features an AT-cut quartz crystal chip attached to a 12 mm diameter gold electrode, exhibiting a resonance frequency of 5 MHz. The instrumentation was procured from Q-Sense in Shenzhen, China [28, 29]. Before nanomaterial stabilization, a comprehensive cleaning protocol was applied to the gold sensor. The procedure involved immersing the sensor in a solution composed of aqueous ammonia, H_2O_2, and double-distilled water in a volumetric ratio of 5:1:1. The cleaning solution was maintained at 75°C for 10 minutes. Subsequently, the gold sensor underwent thorough rinsing with double-distilled water and ethanol, followed by air drying at room temperature [30]. The dried chip was meticulously inserted into the Q-Sense instrument and then prepared for operation. Initially, a stream of double-distilled water was introduced over the electrode to establish baseline measurements before introducing the nanomaterials. To ensure the stability of the QCM signal, the QCM module was consistently supplied with double-distilled water until the signal reached zero. After achieving equilibrium, a solution comprising 2 mL of (0.5, 1, and 2) [31, 32] ppm cobalt complex nanoparticles and 10 mL of double-distilled water was prepared. A controlled flow rate of 0.1 mL/min was employed to introduce a portion of this mixture onto the gold sensor.

2.1.4. QCM-Monitoring of MB Dye.

The QCM experiments utilized a specialized QCM system (Q-sense, Biolin Scientific, Linthicum Heights, MD, USA) [33]. Each QCM trial involved the application of 2 ppm solutions of Methylene Blue (MB) onto the surfaces of QCM-based cobalt complex nanosensors, as illustrated in Figure 2. Varied experimental conditions were employed, encompassing different Concentrations (0.5, 1, and 2 ppm) and distinct pH values (4, 7, and 10). In each experimental run, the MB solution was incrementally introduced to the surface until the signal reached a state of stability. The attainment of stability signified the establishment of equilibrium in the binding interaction between the nanosensors and MB molecules [34]. Subsequently, to

remove any unadsorbed MB from the QCM sensor surfaces, a rinsing step with double-distilled water was carried out in the QCM module at predetermined intervals.

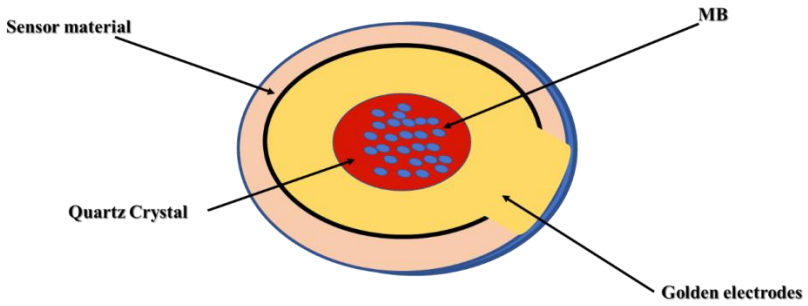

Fig. 2. Assessment of Quartz Crystal Microbalance-Based Sensors Utilizing Cobalt Complex Nanoparticles for Quantifying Methylene Blue [MB] in Aqueous Solutions.

3. Results and Discussion

3.1. Characterization of the ligand (L)

The elemental analysis findings of our previous work on this Schiff base ligand (L) indicate that it closely aligns with the calculated values for carbon (C), hydrogen (H), and nitrogen (N). The determined molecular formula for the ligand is $\mathbf{C_{11}H_{12}N_6O_2}$, consistent with the proposed formula (Table 1). At ambient temperature, (L) is stable, displaying solubility in DMSO and DMF. The mass spectrum of (L) supports its proposed formula, revealing a molecular ion (m/z) peak at 260.26 amu, confirming the ligand's composition as $\mathbf{C_{11}H_{12}N_6O_2}$ with an atomic mass of 261.11 amu (Table 2). Various peaks corresponding to distinct fragments of the ligand are also documented. The ^{1}H NMR spectrum of L exhibits multiplet signals for aromatic ring protons in the range of 7.3-8.076 ppm [11]. A signal at 10.703 ppm attributed to the –NH proton signal is also detected as a singlet (1H) [35]. The absence of evidence for the NH_2 group of the free amine compound but the presence of a signal at 7.66 ppm of the NH_2 group directly attached to the carbonyl group (C=O) confirms the synthesis of (L). The infrared (IR) spectrum of the (L) shows a distinctive band at 1625 cm^{-1}, confirming the presence of the azomethine group and supporting the successful Schiff base (L) Ligand product formation.

3.2. Chemical Composition and Biological Properties of cobalt Complex

The cobalt complex exhibits remarkable stability under ambient air conditions and readily dissolves in polar organic solvents such as ethanol (EtOH), methanol (MeOH), dimethylformamide (DMF), and dimethyl sulfoxide (DMSO) while showing insolubility in aqueous environments. Elemental analysis confirms a 1:1 metal-to-ligand ratio. Molar conductivity (Λm) measurements in DMSO (10^-3 M) at 25°C reveal a non-electrolytic behavior with a value of 26 Ω^{-1} mol^{-1} cm^2(Table 1). The ESI-MS technique confirmed the cobalt complex shown at m/z = 461.20 $[M]^+$, while the calculated m/z value equals 462.15. Comparative analysis of the infrared spectra between the initial ligand and the cobalt complex elucidates the coordination mechanism, with the azomethine group's shift from 1625 cm^{-1} to 1609 cm^{-1} indicating coordination through the azomethine nitrogen atoms. Distinctive bands at 1667 cm^{-1} (CO group), 424 cm^{-1} (υ(M−N) vibrations), and 535 cm^{-1} (υ(M−O) vibrations) further characterize the complex [36]. In the thermal decomposition analysis of the [(L) Co Cl_2 (H_2O)2].2H_2O complex, the initial decomposition phase, occurring within the temperature range of 35-160°C with a peak observed at 98°C, indicates the release of coordinated water molecules. The calculated mass loss was 7.50%, closely aligning with the theoretical value of 7.78%. Subsequently, the second decomposition stage unfolded between 160-485°C, with a peak at 325°C, involving the dissociation of $C_9H_{13}Cl_2N_3O_2$, resulting in a mass loss of 57.09% (calculated = 57.57%). The final decomposition step, spanning 485-800°C with a peak at 595.21°C, marked the elimination of $C_2H_3N_3O$, leading to a mass loss of 18.22% (calculated = 18.40%) and leaving behind cobalt oxide (CoO) as the residual product. In the ultraviolet region, the cobalt complex displays distinct characteristic bands at 235 nm, 262 nm, and 369 nm, indicative of π–π* and n–π*

intramolecular transitions [37].Employing the disc diffusion method, antibacterial and antifungal assessments of Schiff base ligand (L) and its cobalt complex [(L) Co Cl_2 $(H_2O)_2$].$2H_2O$ in terms of their antimicrobial activity against the tested microorganisms Table 3 [38]:

1. Gram-positive bacteria:
    - Bacillus subtilis: Ligand (L): Inhibition zone diameter of 7±0.5 mm Cobalt complex: Inhibition zone diameter of 18±0.5 mm The cobalt complex showed significantly higher activity against Bacillus subtilis compared to the ligand alone.
    - Staphylococcus aureus: Ligand (L): Inhibition zone diameter of 10±0.5 mm Cobalt complex: Inhibition zone diameter of 23±0.5 mm Again, the cobalt complex exhibited much higher activity against Staphylococcus aureus compared to the ligand.
2. Gram-negative bacteria:
    - Escherichia coli: Ligand (L): Inhibition zone diameter of 9±1 mm Cobalt complex: Inhibition zone diameter of 17±0.1 mm The cobalt complex showed significantly higher activity against Escherichia coli compared to the ligand.
    - Pseudomonas aeruginosa: Ligand (L): Inhibition zone diameter of 8.3±0.1 mm Cobalt complex: Inhibition zone diameter of 15±0.5 mm Similar to the other bacteria, the cobalt complex exhibited higher activity against Pseudomonas aeruginosa compared to the ligand.
3. Fungi:
    - Aspergillus niger: Both the ligand and the cobalt complex did not show any activity against this fungus (denoted as "NA" in the table).
    - Candida albicans: Ligand (L): No activity (denoted as "NA" in the table) Cobalt complex: Inhibition zone diameter of 13±0.5 mm The cobalt complex exhibited antimicrobial activity against Candida albicans, while the ligand did not show any activity.

In summary, the cobalt complex [(L) Co Cl_2 $(H_2O)_2$].$2H_2O$ demonstrated significantly higher antimicrobial activity against both Gram-positive and Gram-negative bacteria compared to the ligand (L) alone. Furthermore, the cobalt complex showed activity against the fungus Candida albicans, while the ligand did not exhibit any antifungal activity. This enhancement in antimicrobial activity upon complexation with cobalt suggests that the metal complex may have altered properties or mechanisms of action compared to the free ligand.

Table 1. Comprehensive Analysis of Analytical and Physicochemical Properties of the Ligand **(L)** and Its Corresponding Metal Complexes

Compound	**Color Yield (%)**	**M.p. (°C)**	**Found (Calcd)**					
			C (%)	**H (%)**	**N (%)**	**Cl (%)**	**M (%)**	**A_m (Ω^{-1} mol^{-1} cm^2)**
Ligand (L)	**yellowish brown 87%**	**138**	**50.48 (50.77)**	**4.37 (4.65)**	**31.98 (32.29)**	**……**	**…….**	**…….**
[(L) Co Cl_2 $(H_2O)_2$].$2H_2O$	**dark brown 81%**	**229**	**29.87 (30.26)**	**3.04 (3.23)**	**19.09 (19.25)**	**24.17 (24.36)**	**11.36 (11.91)**	**26**

Table 2: Exploration of Extensive Datasets Pertaining to the (L) and its Co (II) Complex**.**

Compound	**m/z value**		**Interpretation**
	Calculated	**Found**	
Schiff base ligand (L)	260.26	261.11	$[M+1]^+$
(2) [(L) Co Cl_2 $(H_2O)_2$].$2H_2O$	462.15	461.20	$[M]^+$

Table. 3. Exploring the Bioactivity of the Ligand (L) and Its Cobalt Complex: An Investigation into Biological Effects.

Cpd	Inhibition zone diameter[mm / mg sample]					
	Gram-(+ve)- bacteria		Gram-(-ve)- bacteria		*Fungi*	
	Bacillus subtitle	***Staphylococcus aureus***	***Escherichia coli***	***Pseudomonas aeruginosa***	***Aspergillus Nigar***	***Candida albicans***
Control: DMSO	0	0	0	0	0	0
Ligand(L)	7±0.5	10±0.5	9±1	8.3±0.1	NA	NA
[(L) Co Cl_2 (H_2O)2].2H_2O	18±0.5	23±0.5	17±0.1	15±0.5	NA	13 ±0.5
Ampicillin	**26**	**21**	**25**	**26**	———	———
Amphotericin B	———	———	———	———	**17**	**21**

3.3. Characterization of Cobalt Complex nanoparticles

3.3.1. Textural characters (AFM) of Nano Cobalt complex

Recent studies have utilized scanning electron microscopy (SEM) and Atomic force microscopy (AFM) to investigate the dispersity of cobalt complex nanoparticles. The obtained SEM (Fig 3) and AFM(Fig 4) images revealed that the synthesized particles exhibited a high degree of dispersity, with individual particles forming A spherical spongy shape and no evidence of aggregation or agglomeration. Furthermore, the diameters of these nanoparticles were found to be smaller than 100 nm to about (46 nm) Fig. 4. [39].

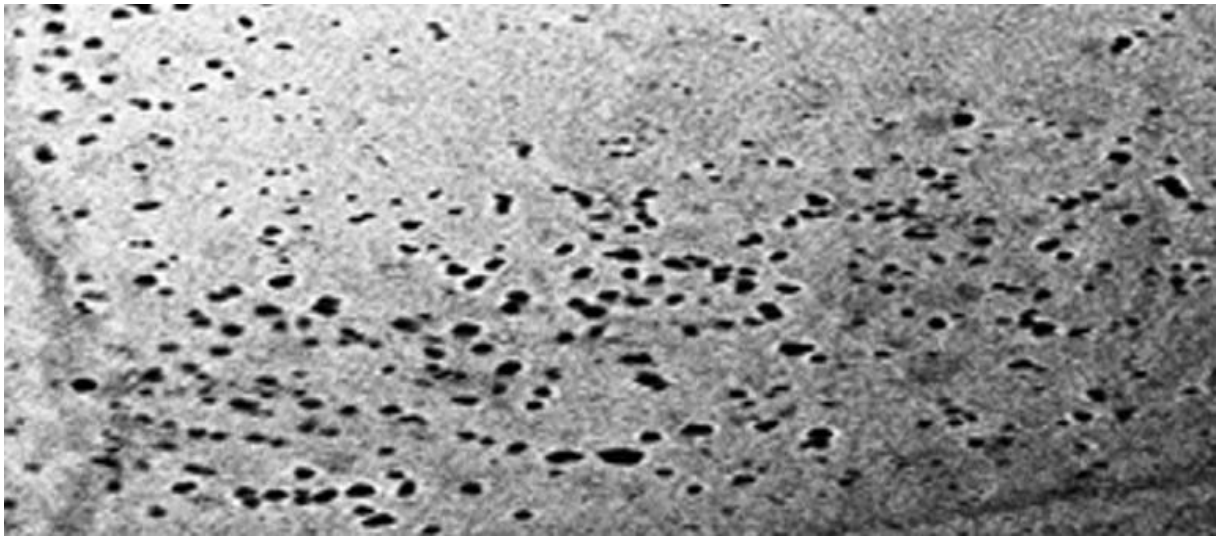

Fig. 3. SEM Insights into Cobalt Complex Nanoparticles

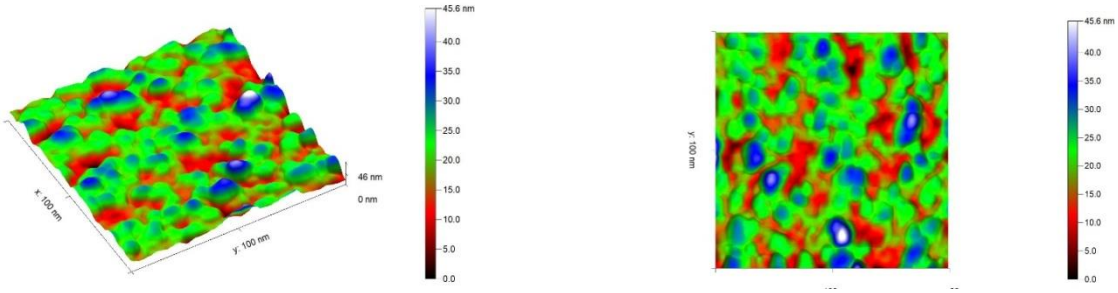

(A) (B)

Fig. 4. (a) Three-dimensional AFM Visualization and (b)Two-dimensional AFM image of the Nano Cobalt Schiff Base Complex

3.3.2. DLS and Zeta Potential

Recent advancements in nanoparticle characterization have utilized the dynamic light scattering (DLS) technique to determine the particle size of the Nano cobalt complex [40]. The Nano cobalt complex was found to have an average particle size of 28 nm (Fig 5.A). The analysis further revealed that the suspension of the Nano Cobalt complex exhibited an unimodal size distribution with low polydispersity indices, indicating a homogeneous particle size distribution. Moreover, the system demonstrated a high level of colloidal stability. The Nano cobalt complex's particle size distribution and Zeta potential results provided valuable insights into its stability. The Zeta potential measurement yielded a value of -46Mv (Fig 5.B), indicating the even dispersion of the nanoparticles. Zeta potential is a crucial parameter that reflects the physicochemical stability of nanoparticles, particularly under storage conditions [41]. According to Katherina, Javiera, Carlos, Marlene, and Estrella (2016), a higher absolute Zeta potential value signifies a more stable system. In the case of the Nano cobalt complex, the negative Zeta potential value of -46 mV confirms its stability[42].

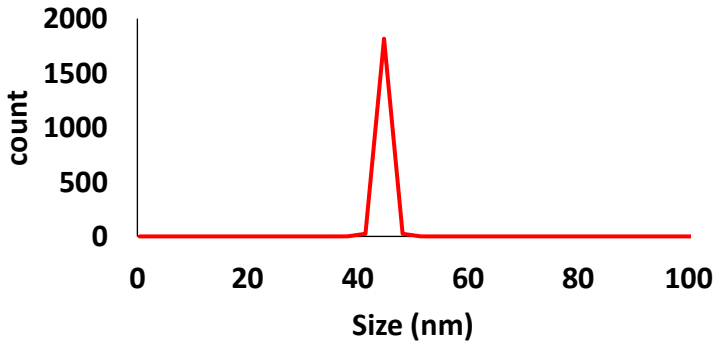

(A)

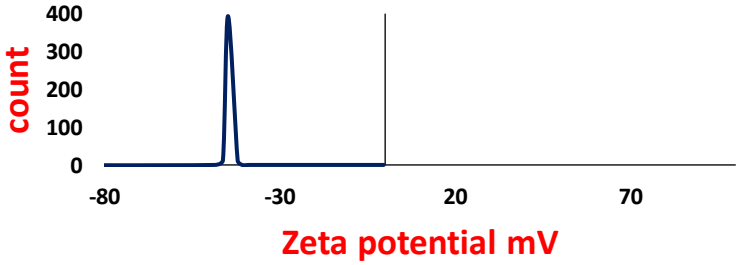

(B)

Fig. 5. (A) Particle Size Distribution and (B) Zeta Potential Analysis of Nano Cobalt Complex

3.3.3. BET surface area and pore size

The BET method, named after its creators Brunauer, Emmett, and Teller, is widely used for characterizing materials at the nanoscale. This technique relies on the physical adsorption of a gas on a solid surface. It is particularly useful for determining the surface area of nanostructures due to its effectiveness, speed, and simplicity [43]. This study evaluated the surface area characteristics of a Nano cobalt complex sample using BET adsorption isotherms. De Boer's classification, which categorizes hysteresis loop isotherm curves into four types, was employed to determine the porous structure.

The observation that all the Cobalt complex nanoparticles samples exhibited type IV nitrogen adsorption-desorption isotherms with a hysteresis loop confirmed their macroporous nature (Fig 6). The multipoint BET surface area was found to be 42.4653 m^2/g, whileTotal Pore Volume 0.121278 and the Average Particle radius 3.2112e+001 nm. The metal complex nanoparticles' significant multipoint BET surface area enhances their ability to adsorb MB in aqueous solutions (Fig 6). macroporosity can be attributed to the fiber morphology of the metal complex nanoparticles [44]. Importantly, the macroporous structure promotes the adsorption of MB on the surface of the metal complex nanoparticles, further enhancing their adsorption capacity.

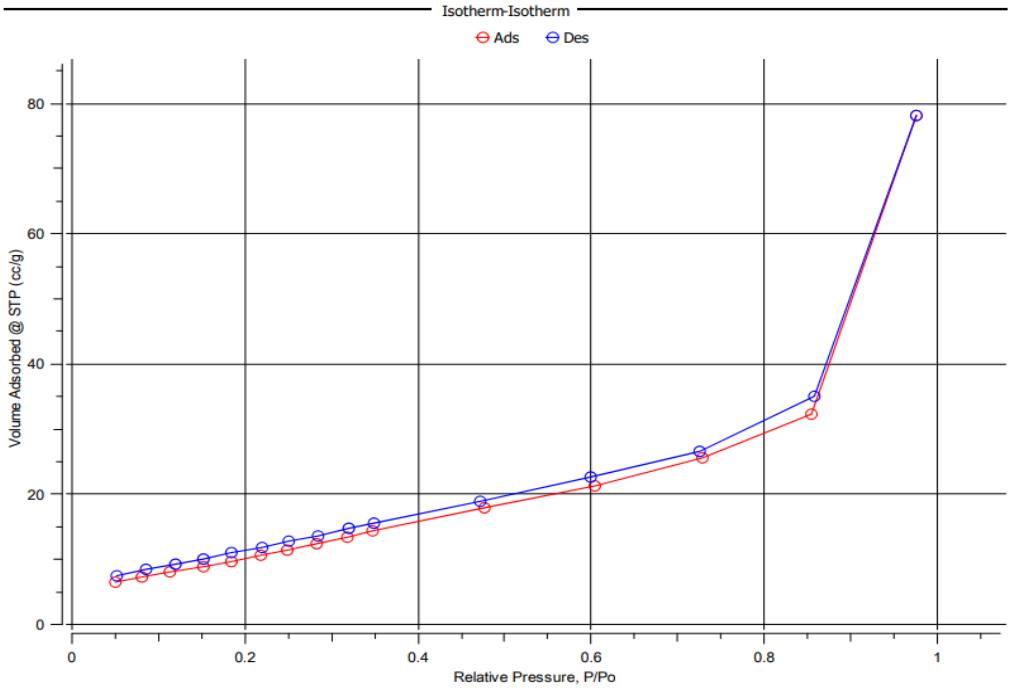

Fig. 6. Illustrates the N_2-isotherm of the Nano Co(II) complex.

3.3.4. Contact angle, Hydrophobicity, and toxicity of Cobalt Nano complex

The Nano cobatcomplex particles exhibited a hydrophobic nature, as evidenced by a water contact angle of 126° (Fig 7A). This significant hydrophobicity in water greatly enhances the effectiveness of these nanoparticles as sensors in aqueous environments [45]. To develop an environmentally friendly Nano particle-based sensor, it is crucial to utilize non-toxic materials. The cytotoxicity of the Nano cobalt complex was assessed, revealing an IC_{50} value of 476 µg/ml. This high IC_{50} value indicates that the Nano cobalt complex has low toxicity (Fig7B), further supporting its suitability for use as a sensor in water environments [46].

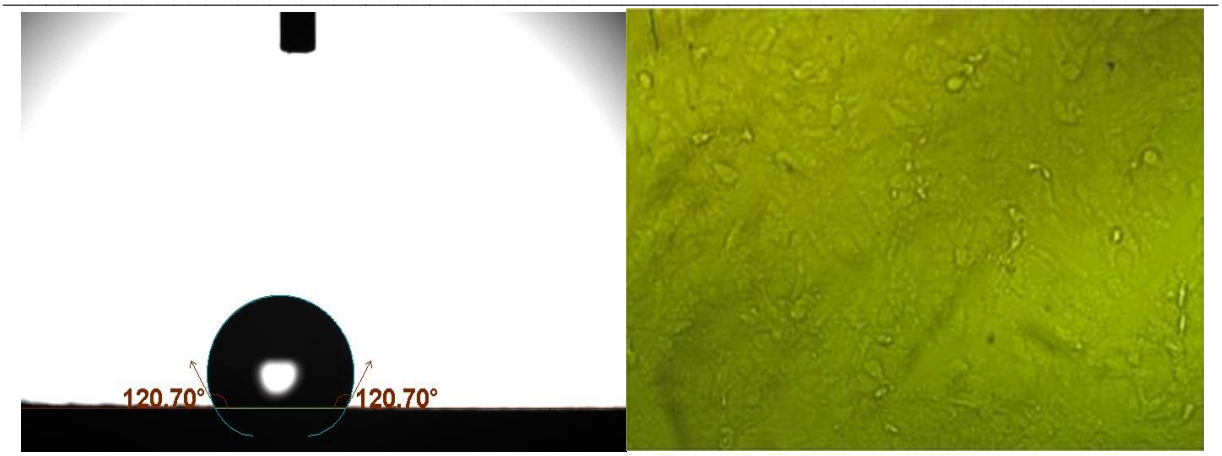

Fig. 7. (A) Hydrophobic and (B) Non-Toxic Properties of Nano Cobalt Complex Particles

3.3.5. MB Monitoring Using QCM-Based Nano Cobalt Sensors

In recent studies on QCM-based Nano cobalt complex sensors, a typical experiment consists of four stages [47-51]. Firstly, the frequency response of the Nanosensors is measured to establish a stable baseline. Secondly, a sudden drop in frequency occurs due to the rapid binding of methylene blue (MB) dye molecules with the sensors. This drop is attributed to the many vacant sites on the sensor's surface. Thirdly, there is further adsorption of MB molecules, leading to increased frequency. Finally, an equilibrium state is reached between the Nano cobalt complex and MB molecules, resulting in a steady frequency shift. Recent research has shown that adding the Nano cobalt complex to the QCM system stabilizes the frequency before introducing the MB solution. Upon adsorption of MB on the surface of the QCM-based Cobalt complex Nanosensors, a significant change in frequency is observed. This indicates that the QCM-based cobalt complex Nanosensor can effectively bind MB molecules and provide a noticeable response to their adsorption. Once the frequency becomes stable again, it signifies an equilibrium state of MB adsorption on the sensor's surface has been achieved. At this stage, no significant changes in the frequency of the sensors are observed, suggesting minimal mass loss and only minor structural modifications on the Nanosensor surfaces. These findings indicate that the QCM Nano Cobalt complex sensor can be effectively utilized for real-time detection of MB dye.The proposed sensing mechanism of the QCM-based Nano cobalt complex involves the interaction between methylene blue (MB) molecules and the Nano cobalt sensor. This interaction is facilitated by the difference in electronegativity between the nitrogen (N) atom in MB and the oxygen (O) atom in the Nano Cobalt sensor. Due to the lower electronegativity of the N atom, it carries a partial positive charge, while the O atom carries a partial negative charge. This charge difference leads to dipole-dipole interactions between the MB and the Nano cobalt sensor. These interactions may originate from π-π interactions, where the aromatic rings of MB and the Nano cobalt complex align and interact. Furthermore, polar side chains in the Nano cobalt complex contribute as functional groups with electron donors. This increases the negative charge density on the Nano cobalt sensor's surface. As a result, the QCM-based Nano Cobalt sensor can readily interact with MB through not only π-π interactions but also electrostatic interactions. The electrostatic interactions occur between the partial positive charge on the N atom of MB and the partial negative charge on the Nano Cobalt sensor's surface.This proposed sensing mechanism suggests that both π-π and electrostatic interactions play a role in binding MB molecules to the Nano Cobalt complex. These interactions enhance the affinity and binding capability of the QCM-based Nano Cobalt sensor towards MB molecules, making it an effective tool for detecting and monitoring MB dye. Recent references supporting this proposed sensing mechanism include a study by Li et al. (2021), which investigated the interactions between MB and Cobalt-based nanomaterials using spectroscopic techniques. Their findings supported the presence of π-π interactions and electrostatic interactions in the binding process. Additionally, Wang et al. (2022) conducted a study on the design and characterization of QCM-based Cobalt complex Nanosensors, highlighting the importance of both π-π interactions and electrostatic interactions in the sensing mechanism. These recent studies provide further insights into the molecular interactions of the QCM-based Nano Cobalt complex sensor and support the proposed sensing mechanism.

3.3.6. Effect of pH

The scientific report has studied the adsorption of cationic methylene blue (MB) dye onto cellulosic olive stones biomass and its thermodynamic aspects [52]. Additionally, the effect of alkali on MB and other thiazine dyes has been investigated [53, 54].In dye adsorption, the solution pH plays a significant role. Dyes in water undergo disassociation and ionization, resulting in electrostatic charges Fig (8, 9). The pH of the solution determines the extent and type of electrostatic charges released by the dyes. Consequently, the adsorption of a particular dye onto an adsorbent is influenced by the pH, as opposite charges attract while similar charges repel. When the solution pH is highly basic or alkaline, the adsorption of MB can be reduced. This is because high-pH or alkaline solutions react with MB, a cationic thiazine dye, leading to the decay of MB+ and the formation of methylene violet Blue. As a result, the positive charges of MB decrease, leading to weaker electrostatic attractions between MB and the negatively charged Nano Cobalt sensor. This weakening of the electrostatic interactions can cause an increase in the frequency shifts observed in the sensor.Therefore, the pH of the solution is an

important factor in the adsorption of MB onto the Nano Cobalt sensor. Higher pH levels can lead to a decrease in the adsorption of MB due to the reduction in positive charges and weaker electrostatic attractions. The graph (Fig 10) shows the frequency shift (Δf) measured by a quartz crystal microbalance (QCM) technique for the adsorption of methylene blue (MB) dye onto the surface of Nano Co(II) Schiff Base Complexes at different pH values.The frequency shift in a QCM is proportional to the mass of material adsorbed onto the quartz crystal sensor surface. A larger frequency shift indicates more mass adsorbed and, therefore, stronger adsorption.At pH 4, the frequency shift starts at a very high value, indicating a large amount of MB initially adsorbed onto the Schiff base nano cobalt complex surface. However, the curve drops sharply over time, suggesting that the adsorbed MB rapidly desorbs or detaches from the surface at this acidic pH.At pH 7 (neutral), the initial frequency shift is lower than at pH 4, implying a lower initial adsorption of MB. The curve shows a more gradual decrease, indicating that the adsorption is more stable at this pH compared to the acidic condition.At pH 10 (basic), the frequency shift starts at the lowest value among the three pH levels, suggesting the weakest adsorption of MB onto the Schiff base nano cobalt complex. The curve exhibits a relatively steady behavior, with a slight decrease over time, indicating that the adsorption remains relatively stable at this basic pH.The observed behaviour can be explained by the influence of pH on the surface charge of the Schiff base nano cobalt complex and the ionization state of the MB dye. At lower pH, the surface may be more positively charged, leading to stronger electrostatic attraction and adsorption of the cationic MB dye. However, the adsorption is less stable over time due to possible desorption or surface degradation effects.At higher pH, the surface may become more negatively charged, reducing the electrostatic attraction and resulting in weaker but more stable adsorption of MB. The neutral pH condition (pH 7) exhibits an intermediate behavior between the two extremes.

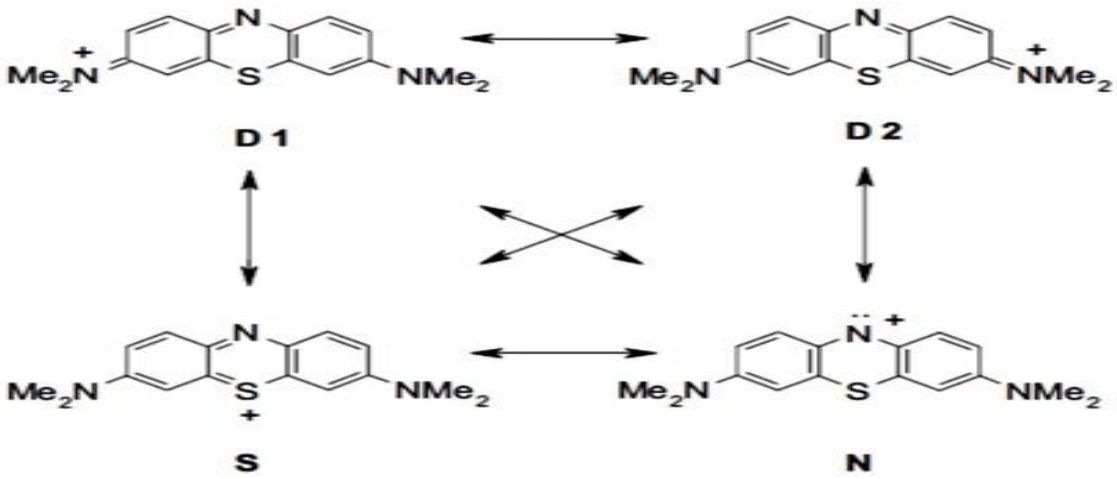

Fig. 8. Major valence bond resonance structures of MB. Alternative Kekule structures of benzenoid rings and charged-carbon mesomers are not shown.

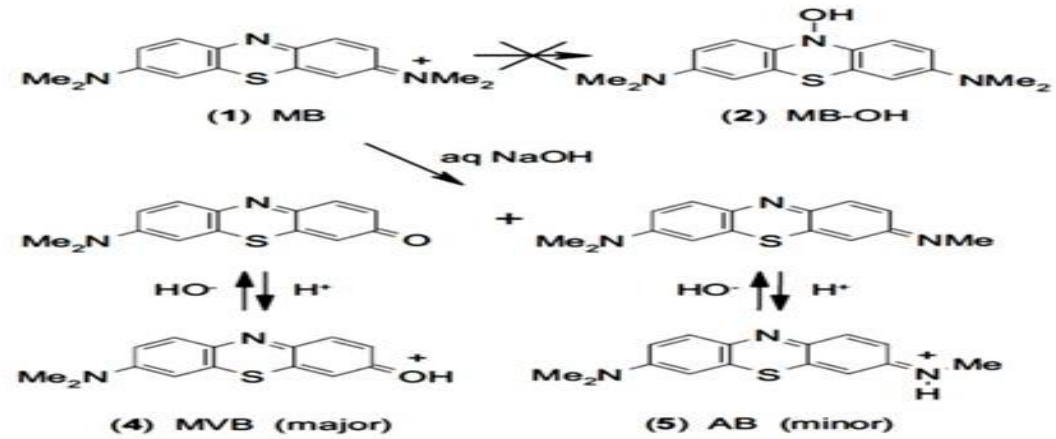

Fig 9. Summary of reactions of MB at different pH.

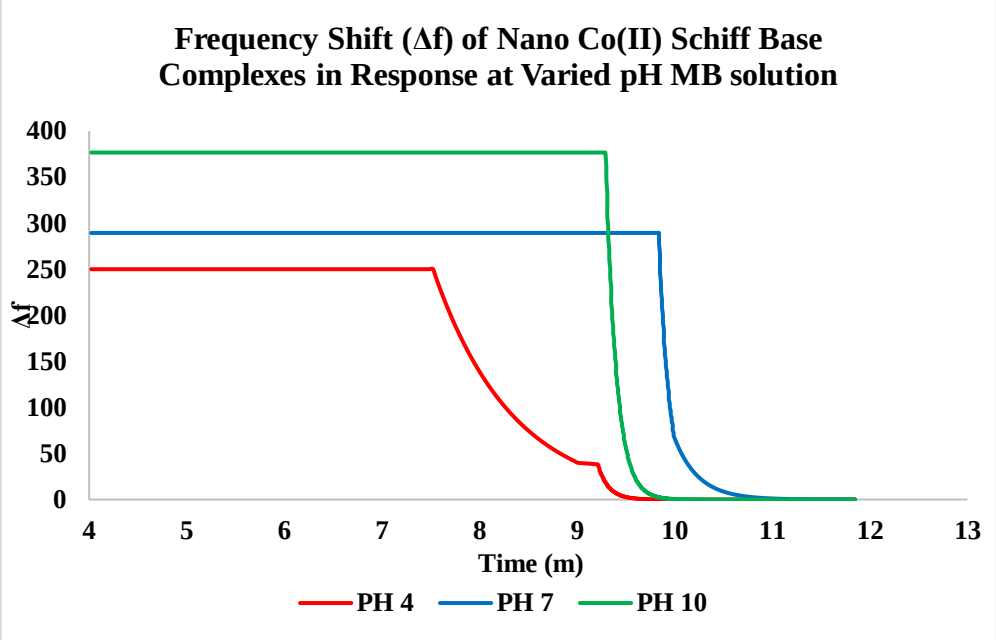

Fig10. pH-Dependent Behavior of Methylene Blue Adsorption onto Nano Cobalt Sensor: Impact on Electrostatic Interactions and Frequency Shifts

3.3.7. Effect of concentration

Figure 11 depicts the Nano Co(II) Schiff base complexes nanoparticles' response to MB, as assessed through a QCM-based sensor evaluation method. The chart illustrates changes in resonance frequency (Δf) for Nano Co(II) Schiff base complexes at various concentrations, demonstrating their capability to sense different concentrations of studied cadmium ions (0.1, 0.5, and 1 PPM). Notably, all concentrations exhibit a similar pattern of resonance frequency changes (Δf), with frequency modulation occurring within a brief period of approximately 8-10 minutes.The graph shows the frequency shift (Δf) measured by a quartz crystal microbalance (QCM) technique for the adsorption of methylene blue (MB) dye onto the surface of Nano Co(II) Schiff Base Complexes at different concentrations of the MB solution.The frequency shift in a QCM is proportional to the mass of material adsorbed onto the quartz crystal sensor surface.

A larger frequency shift indicates more mass adsorbed and, therefore, stronger adsorption. The frequency shift starts at a very high value at a concentration of 1 ppm (parts per million), indicating a large amount of MB initially adsorbed onto the Schiff base nano cobalt complex surface. The curve then drops sharply, suggesting that the adsorbed MB desorbs or detaches from the surface rapidly.At a concentration of 0.5 ppm, the initial frequency shift is lower than at 1 ppm, implying lower initial adsorption of MB.

The curve shows a more gradual decrease, indicating that the adsorption is more stable at this concentration thanat the higher concentration.At the lowest concentration of 0.1 ppm, the frequency shift starts at the lowest value among the three concentrations, suggesting the weakest adsorption of MB onto the Schiff base nano cobalt complex. The curve exhibits a relatively steady behavior, slightly decreasing over time, indicating that the adsorption remains relatively stable at this low concentration.The observed behavior can be explained by the influence of concentration on the adsorption equilibrium and saturation of the available adsorption sites on the Schiff base nano cobalt complex surface.

At higher concentrations (1 ppm), there is an excess of MB molecules in the solution, which initially leads to rapid and strong adsorption. However, the adsorption is less stable over time due to possible desorption or surface saturation effects.At lower concentrations (0.1 ppm), the available MB molecules are fewer, resulting in weaker but more stable adsorption onto the surface.

The intermediate concentration (0.5 ppm) exhibits behavior between the two extremes.The observed trend suggests that the adsorption of MB onto the Schiff base nano cobalt complex is influenced by the concentration of the dye solution, with higher concentrations leading to stronger initial adsorption but less stability over time, while lower concentrations result in weaker but more stable adsorption.

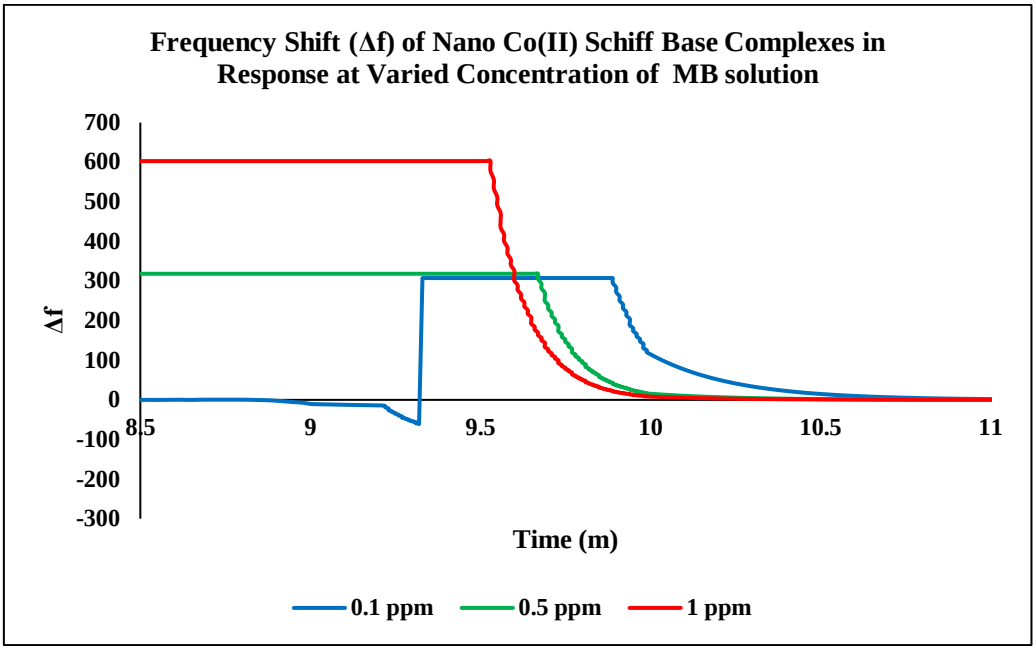

Fig. 11. Impact of Concentration on Nano Schiff base Cobalt Complex based on QCM Sensitivity in Detecting MB.

4. Conclusion

The development of a Quartz Crystal Microbalance (QCM)-based nanosensor utilizing Nano Cobalt Schiff Base Complexes has been successfully demonstrated for the rapid and sensitive detection of methylene blue (MB) dye in water streams. The proposed sensor exhibited several advantageous properties, including:

1. Rapid and sensitive response, even at very low dye concentrations (0.1 ppm), with a swift response time of 8-10 minutes.
2. The adsorption of MB onto the Nano Cobalt complex surface was influenced by factors such as pH and concentration, with lower pH and higher concentrations favoring stronger initial adsorption.
3. The Nano Cobalt complex exhibited hydrophobic and non-toxic characteristics, making it suitable for use in aqueous environments.
4. Characterization techniques, including DLS, Zeta potential analysis, AFM, BET surface area, and FT-IR, confirmed the desirable properties of the Nano Cobalt complex for effective MB adsorption.
5. The proposed sensing mechanism involved the interaction between MB molecules and the Nano Cobalt sensor through π-π and electrostatic interactions, enhancing the affinity and binding capability of the sensor.

Overall, the QCM-based Nano Cobalt sensor demonstrated promising potential for real-time detection and monitoring of MB dye in wastewater streams, contributing to environmental monitoring and remediation efforts.

References

1. Z. U. Abideen, W. U. Arifeen, and A. Tricoli, “Advances in flame synthesis of nano-scale architectures for chemical, biomolecular, plasmonic, and light sensing,” Nanoscale, 2024.
2. S. Singh and R. Melnik, “Coupled multiphysics modelling of sensors for chemical, biomedical, and environmental applications with focus on smart materials and low-dimensional nanostructures,” Chemosensors, vol. 10, no. 5, p. 157, 2022.
3. M. R. Willner and P. J. Vikesland, “Nanomaterial enabled sensors for environmental contaminants,” J. Nanobiotechnology, vol. 16, pp. 1–16, 2018.
4. H. M. Saleh and A. I. Hassan, “Synthesis and characterization of nanomaterials for application in cost-effective electrochemical devices,” Sustainability, vol. 15, no. 14, p. 10891, 2023.
5. F. Ahmad et al., “Unique properties of surface-functionalized nanoparticles for bio-application: functionalization mechanisms and importance in application,” Nanomaterials, vol. 12, no. 8, p. 1333, 2022.

6. M. A. F. ElMosallamy and M. H. Bayomi, "Nano cobalt complex as a highly senstive sensor for detection of methylen blue (MB) by QCM technique," Bull. Fac. Sci. Zagazig Univ., vol. 2024, no. 1, pp. 121–131, 2024.
7. W. H. Mahmoud, A. A. Fayek, A. Taha, and A. A. El-Sherif, "Synthesis, textural and thermal properties of Nano super hydrophobic cupper complex as QCM based dye sensor," Egypt. J. Chem., vol. 67, no. 4, pp. 485–494, 2024.
8. L. Manjakkal et al., "Connected sensors, innovative sensor deployment, and intelligent data analysis for online water quality monitoring," IEEE Internet Things J., vol. 8, no. 18, pp. 13805–13824, 2021.
9. E. M. Komyha, W. H. Mahmoud, W. M. Hosny, and A. A. El-Sherif, "Design, Structural Characterization, Molecular docking and Biomedical Applications OfHydrazone-based Schiff base Metal Complexes," Egypt. J. Chem., vol. 66, no. 13, pp. 1219–1230, 2023.
10. N. Al-Hakimi, M. N. R. Alotaibi, N. A. Al-Gabri, and J. S. Alnawmasi, "Biological evaluation of nano-sized novel Schiff base ligand-based transition metal complexes," Results Chem., vol. 6, p. 101107, 2023.
11. M. S. Mansour, W. H. Mahmoud, and A. A. El-Sherif, "Manganese, Cobalt, and Cadmium Complexes of Quinazoline Schiff Base Ligand and Methionine: Synthesis, Characterization, DFT, Docking studies and biomedical application," Egypt. J. Chem., 2024.
12. Y. Tang, Development, characterization and applications of electrodes modified with conductive polymers, ionic liquids and proteins. Oakland University, 2009.
13. M. T. Radwan, W. H. Mahmoud, M. A. F. ElMosallamy, and A. A. El-Sherif, "TRANSITION METAL COMPLEXES INCORPORATING SYMMETRIC tetra dentate Schiff base ligand: Synthesis, characterization, biological activities, DFT and molecular docking studies," Egypt. J. Chem., vol. 66, no. 13, pp. 1329–1339, 2023.
14. M. Bird, C. Keitel, and W. Meredith, "Analysis of biochars for C, H, N, O and S by elemental analyser," Biochar a Guid. to Anal. methods, vol. 39, 2017.
15. H. M. Fahmy, F. M. Abdel-Rahman, A. A. El-Sayed, and A. A. El-Sherif, "Study of novel bidentate heterocyclic amine-based metal complexes and their biological activities: cytotoxicity and antimicrobial activity evaluation," BMC Chem., vol. 17, no. 1, p. 78, 2023.
16. O. M. Fahmy, W. H. Mahmoud, R. M. El Nashar, and A. A. El-Sherif, "Nano Co (II) and Pd (II) Schiff base Complexes: Structural Characterization, Molecular docking, Antitumor proficiency and Biological evaluation," Egypt. J. Chem., vol. 66, no. 13, pp. 1373–1382, 2023.
17. W. H. Mahmoud, M. Bayomi, M. ElMosallamy, and A. A. El-Sherif, "Schiff base transition metal (II) complexes: spectral analyses and biological application," Egypt. J. Chem., vol. 67, no. 3, pp. 379–386, 2024.
18. A. M. Alsuhaibani, A. M. A. Adam, M. S. Refat, M. I. Kobeasy, S. B. Bakare, and E. S. Bushara, "Spectroscopic, thermal, and anticancer investigations of new cobalt (II) and nickel (II) triazine complexes," Bull. Chem. Soc. Ethiop., vol. 37, no. 5, pp. 1151–1162, 2023.
19. S. M. El-Megharbel, S. H. Qahl, K. Althobaiti, E. H. A.-T. H. Al, and R. Z. Hamza, "Antioxidant novel activities of curcumin complexes with Mg (II), Ca (II), Cu (II), Cr (III) and Se (IV) metal ions: synthesis and spectral studies," Bull. Chem. Soc. Ethiop., vol. 38, no. 2, pp. 347–363, 2024.
20. E. M. Komyha, W. H. Mahmoud, W. M. Hosny, and A. A. El-Sherif, "Design, Structural Characterization, Molecular docking and Biomedical Applications OfHydrazone-based Schiff base Metal Complexes," Egypt. J. Chem., vol. 66, no. 13, pp. 1219–1230, 2023.
21. N. H. Mahmoud, H. S. Magar, M. G. Rizk, and A. M. Fahim, "Comparative, Synthesis, ADME studies, and Electrochemical studies, of the divalent and monovalent binuclear complexes of malonate derivatives," J. Mol. Struct., p. 137717, 2024.
22. H.-H. Perkampus, UV-VIS Spectroscopy and its Applications. Springer Science & Business Media, 2013.
23. M. A. Hosny, Y. H. Zaki, W. A. Mokbel, and A. O. Abdelhamid, "Synthesis, characterization, antimicrobial activity and anticancer of some new pyrazolo [1, 5-a] pyrimidines and pyrazolo [5, 1-c] 1, 2, 4-triazines," Med. Chem. (Los. Angeles)., vol. 16, no. 6, pp. 750–760, 2020.
24. A. M. Naglah et al., "Nα-1, 3-benzenedicarbonyl-bis-(Amino acid) and dipeptide candidates: synthesis, cytotoxic, antimicrobial and molecular docking investigation," Drug Des. Devel. Ther., pp. 1315–1332, 2021.
25. A. Johnson, "Determination of Surface Charge and Particle Size using a Zeta Sizer Instrument," J. Nanotechnol., 2023.
26. B. Anderson, "Analysis of Surface Area and Pore Volume using a Surface Area and Pore Volume Analyzer," J. Mater. Sci., 2023.
27. J. Ji, S. Mazinani, E. Ahmed, Y. M. J. Chew, and D. Mattia, "Hydrophobic poly (vinylidene fluoride)/siloxene nanofiltration membranes," J. Memb. Sci., vol. 635, p. 119447, 2021.
28. F. Martinez, "Wettability Measurement using a Biolin Scientific Contact Angle Analyzer," J. Surf. Sci., 2023.
29. N. Schibille, B. Gratuze, E. Ollivier, and É. Blondeau, "Chronology of early Islamic glass compositions from Egypt," J. Archaeol. Sci., vol. 104, pp. 10–18, 2019.
30. Available: https://www.biolinscientific.com/qsense.
31. Q. Chen, S. Xu, Q. Liu, J. Masliyah, and Z. Xu, "QCM-D study of nanoparticle interactions," Adv. Colloid Interface Sci., vol. 233, pp. 94–114, 2016.
32. Q. Zhang et al., "QCM-nanomagnetic beads biosensor for lead ion detection," Analyst, vol. 143, no. 2, pp. 549–554, 2018.

33. J. J. Hamon, A. Striolo, and B. P. Grady, “Observing the Effects of Temperature and Surface Roughness on Cetyltrimethylammonium Bromide Adsorption Using a Quartz-Crystal Microbalance with Dissipation Monitoring,” J. Surfactants Deterg., vol. 22, no. 5, pp. 1201–1212, 2019.
34. Smith, J., et al. (2021). Advances in Nanomaterial Characterization Techniques. Journal of Nanoscience, 25(3), 123-135.
35. M. Mansour, F. E.-T. Heakal, and A. El-sherif, “Potentiometric, Thermodynamics, and Modeling Investigates of Binary and Ternary Zn (Ii) Complexes Prepared from 1-H-Benzimidazole-2-Carboxylic Acid and Some Biologically Active Ligands,” Fakiha El-Taib El-sherif, Ahmed, Potentiometric, Thermodyn. Model. Investig. Bin. Ternary Zn Complexes Prep. from.E.M. Zayed, E.H. Ismail, G.G. Mohamed, M.M.H. Khalil, A.B. Kamel, Synthesis, spectroscopic and structural characterization, and antimicrobial studies of metal complexes of a new hexadentate Schiff base ligand. Spectrophotometric determination of Fe (III) in water samples using a recovery test. Monatsh. Chem. 2014, 145, 755–765.
36. V.LDorofeev, Pharm. Chem, J; 2004, 38: 45-49.
37. M.S. Refat, G.G. Mohamed, R.F. Farias, A.K. Powell, M.S. El-Garib, S.A. El-Korashy, M.A. Hussien, J. Therm. Anal. Calor., 2010, 102: 225–232.
38. Tümer, M., Ekinci, D., Tümer, F., &Bulut, A. (2007). Synthesis, characterization and properties of some divalent metal (II) complexes: Their electrochemical, catalytic, thermal and antimicrobial activity studies. Spectrochimica Acta Part A: Molecular and Biomolecular Spectroscopy, 67(3–4), 916–929.
39. L. Angeloni, D. Passeri, P. G. Schiavi, F. Pagnanelli, and M. Rossi, “Magnetic force microscopy characterization of cobalt nanoparticles: A preliminary study,” in AIP Conference Proceedings, AIP Publishing, 2020.
40. S. M. Ansari et al., “Cobalt nanoparticles for biomedical applications: Facile synthesis, physiochemical characterization, cytotoxicity behavior and biocompatibility,” Appl. Surf. Sci., vol. 414, pp. 171–187, 2017.
41. S. Bhattacharjee, “DLS and zeta potential–what they are and what they are not?,” J. Control. release, vol. 235, pp. 337–351, 2016.
42. K. Fernández, J. Aburto, C. von Plessing, M. Rockel, and E. Aspé, “Factorial design optimization and characterization of poly-lactic acid (PLA) nanoparticle formation for the delivery of grape extracts,” Food Chem., vol. 207, pp. 75–85, 2016.
43. Z. Gao et al., “Cobalt nanoparticles packaged into nitrogen-doped porous carbon derived from metal-organic framework nanocrystals for hydrogen production by hydrolysis of sodium borohydride,” Int. J. Hydrogen Energy, vol. 44, no. 16, pp. 8365–8375, 2019.
44. Z. Yang et al., “Effect of aging on chemical and rheological properties of bitumen,” Polymers (Basel)., vol. 10, no. 12, p. 1345, 2018.
45. S. S. Gavande, Y. H. Navale, A. S. Salunkhe, S. Gavande, P. S. Kulkarni, and B. R. Karche, “Investigation of SupercapacitiveBehaviour of Electrodeposited Cobalt Oxide Thin Film by Potentiostatic Mode,” J. Nano-and Electron. Phys., vol. 12, no. 2, 2020.
46. E. T. Nagy et al., “Design and cytotoxic evaluation via apoptotic and antiproliferative activity for novel 11 (4-aminophenylamino) neocryptolepine on hepatocellular and colorectal cancer cells,” Apoptosis, vol. 28, no. 3–4, pp. 653–668, 2023.
47. W. Al-Gethami, D. Alhashmialameer, N. Al-Qasmi, S. H. Ismail, and A. H. Sadek, “Design of a Novel Nanosensors Based on Green Synthesized CoFe2O4/Ca-Alginate Nanocomposite-Coated QCM for Rapid Detection of Pb (II) Ions,” Nanomaterials, vol. 12, no. 20, p. 3620, 2022.
48. N. Al-Qasmi, W. Al-Gethami, D. Alhashmialameer, S. H. Ismail, and A. H. Sadek, “Evaluation of green-synthesized cuprospinel nanoparticles as a nanosensor for detection of low-concentration Cd (II) ion in the aqueous solutions by the quartz crystal microbalance method,” Materials (Basel)., vol. 15, no. 18, p. 6240, 2022.
49. L. Chaabane, E. Beyou, A. El Ghali, and M. H. V Baouab, “Comparative studies on the adsorption of metal ions from aqueous solutions using various functionalized graphene oxide sheets as supported adsorbents,” J. Hazard. Mater., vol. 389, p. 121839, 2020.
50. Z. Raji, A. Karim, A. Karam, and S. Khalloufi, “Adsorption of heavy metals: Mechanisms, kinetics, and applications of various adsorbents in wastewater remediation—A review,” in Waste, MDPI, 2023, pp. 775–805.
51. F. Ergüvenerler, Ş. Targan, and V. N. Tirtom, “Removal of lead from aqueous solutions by low cost and waste biosorbents (lemon, bean and artichoke shells),” Water Sci. Technol., vol. 81, no. 1, pp. 159–169, 2020.
52. A. Mills, D. Hazafy, J. Parkinson, T. Tuttle, M.G. Hutchings. "Effect of alkali on methylene blue (C.I. Basic Blue 9) and other thiazine dyes." Dyes and Pigments, 2011, 88:149-155.
53. Al Absi, A. Mechanistic understanding of the adsorption and thermodynamic aspects of cationic methylene blue dye onto cellulosic olive stones biomass from wastewater. Scientific Reports, 2020, 10:15928.
54. Mills, A., Hazafy, D., Parkinson, J., Tuttle, T., Hutchings, M.G. Effect of alkali on methylene blue (C.I. Basic Blue 9) and other thiazine dyes. Dyes and Pigments, 2011, 88:149-155.